

Time reversal breaking of colloidal particles in cells

Gabriel Knotz,¹ Till M. Muenker,² Timo Betz,² and Matthias Krüger¹

¹*Institute for Theoretical Physics, University of Göttingen, 37077 Göttingen, Germany*

²*Third Institute of Physics, University of Göttingen, 37077 Göttingen, Germany*

(Dated: March 18, 2026)

We investigate signatures of broken time reversal symmetry in stochastic trajectory data, employing the previously introduced three point correlation called mean back relaxation. We specifically investigate data from a simple driven model, as well as from colloidal particles within living or passivated biological cells. Both in the model as well as in cell data, MBR detects broken time reversal symmetry, and furthermore, allows to determine relevant time and length scales of activity. For the cells, we show, by applying various drugs, that it is predominantly the presence of microtubules which is needed for a time reversal symmetry breaking. We employ a bound for entropy production, finding that it is in striking relation to previously determined active energies that quantify violation of the fluctuation dissipation theorem.

I. INTRODUCTION

The study of non-equilibrium processes is a vibrant and growing field of research in physics as well as biophysics. A key challenge in this field is determination of signatures that distinguish equilibrium from non-equilibrium systems. Finding such signatures can be particularly challenging when dealing with highly coarse-grained dynamics, such as, e.g., colloidal particles in complex environments^{1,2}. There are various established signatures. A standard method³⁻⁶ is testing the validity of the fluctuation-dissipation theorem (FDT)⁷⁻¹³, whose violations are considered a signal for non-equilibrium. This procedure however requires measuring the system's mechanical response, for example, using optical or magnetic tweezers¹⁴⁻¹⁶. This can be experimentally challenging, as perturbations must be small to stay in the linear response regime. Another direct signature is the observation of probability currents as indicators of non-equilibrium processes^{17,18}, or the breakage of time reversal symmetry¹⁹. Formally, the latter is quantified by entropy production, for which various theorems exist²⁰⁻²². Entropy production is typically hard to measure directly, and recent years have seen the developments of bounds for it, e.g., in terms of moments of currents or time-antisymmetric observables²³⁻²⁸ or by other methods²⁹⁻³¹.

In this manuscript, we demonstrate that stochastic trajectories of Brownian particles immersed in living cells break time reversal symmetry, thereby demonstrating the non-equilibrium nature by purely passive observation³². The investigation utilizes the mean back relaxation (MBR), a recently introduced observable³³⁻³⁵ based on three time points. MBR contains a path anti-symmetric part which is used to detect time reversal symmetry breaking, and which also allows to infer the length and time scales on which this symmetry is predominantly broken. Finally, we employ a previously derived bound for entropy production, thus providing a lower bound of entropy production in living cells. The so found bound is in qualitative agreement with previously determined active energies. We generalize the previously introduced

random horse and cart model³⁵ to a non-Gaussian version to allow for time reversal symmetry breaking. The model allows to illustrate the findings observed in cells.

The manuscript is organized as follows. In Section II we briefly introduce MBR. In Section III we investigate a model system that exhibits time reversal breaking, which is detected by MBR, and we investigate how MBR can be used to determine the time and length scales of predominant breaking of time reversal symmetry. In Section IV we apply MBR to cell data and demonstrate that it detects time reversal breaking for multiple different cell types. By investigating drugged cell types, we find that the time reversal breaking is primarily caused by processes associated with microtubules. Finally, in Section V, we apply an entropy production bound and demonstrate qualitative agreement between the bound and a previously determined active energy.

II. MEAN BACK RELAXATION

We define mean back relaxation (MBR) for a stochastic variable $x(t)$ as the average of the negative ratio between the displacements $x(t) - x(0)$ and $x(0) - x(-\tau)$, with $\tau > 0$, i.e.,

$$\begin{aligned} \text{MBR}(\tau, t, l) &= - \left\langle \frac{x(t) - x(0)}{x(0) - x(-\tau)} \vartheta_l(x(0) - x(-\tau)) \right\rangle \\ &= \int dx_t dx_0 dx_{-\tau} \left(- \frac{x_t - x_0}{x_0 - x_{-\tau}} \right) \\ &\quad \times \vartheta_l(x_0 - x_{-\tau}) W_3(x_t, t; x_0, 0; x_{-\tau}, -\tau), \end{aligned} \quad (1)$$

$W_3(x_{t_3}, t_3; x_{t_2}, t_2; x_{t_1}, t_1)$ is the joint three-point probability of finding the particle at positions $x_{t_3}, x_{t_2}, x_{t_1}$ at times $t_3 > t_2 > t_1$. The factor $\vartheta_l(x(0) - x(-\tau)) \equiv \frac{\theta(|x(0) - x(-\tau)| - l)}{Z}$ with the Heaviside function $\theta(x)$, $Z = \langle \theta(|x(0) - x(-\tau)| - l) \rangle$ and a length $l > 0$ avoids division by zero in Eq. (1). By construction, it is normalized to unity, i.e., $\langle \vartheta_l(x(0) - x(-\tau)) \rangle = 1$, and the length l is the smallest value of $|x_0 - x_{-\tau}|$ considered in Eq. (1), i.e.,

a cutoff length. We introduced a minus sign in Eq. (1) to obtain a positive result for MBR in the case of back relaxation, i.e., when the displacements have opposite signs. MBR depends on the mentioned cut off length l , and the two times t and τ at which the displacements in Eq. (1) are evaluated.

MBR has been proven to be a marker of time reversal symmetry breaking³⁴: Under the condition that the mean $\langle x \rangle$ exists and is approached in finite time, one has, for a process obeying detailed balance,³⁴

$$\lim_{t \rightarrow \infty} \text{MBR}(\tau, t, l) = \frac{1}{2}, \quad (2)$$

independent of τ and l .

We have not been able to demonstrate that the conditions for Eq. (2) are fulfilled for the particle in a cellular surrounding³³, this is why we will not make use of Eq. (2) in this manuscript. Instead, we will evaluate the time anti-symmetric part of MBR, which is distilled by taking the difference between MBR evaluated from forward and backward trajectories

$$\text{MBR}_{\text{anti}}(\tau, t, l) = \left\langle -\frac{x(t+\tau) - x(\tau)}{x(\tau) - x(0)} \vartheta_l(x(\tau) - x(0)) + \frac{x(0) - x(t)}{x(t) - x(t+\tau)} \vartheta_l(x(t) - x(t+\tau)) \right\rangle. \quad (3)$$

Being the average of a path antisymmetric observable, MBR_{anti} must vanish for a time reversal symmetric process. A finite value of MBR_{anti} thus signals breakage of time reversal symmetry. This will be explored for a toy model in Section III and for experimental data obtained in cells in Section IV.

III. MODEL: DISCRETE RANDOM HORSE AND CART

A. Model

We start by investigating MBR_{anti} for a model system. In previous work^{33,35}, we introduced the "random horse and cart" (RHC) model, set out to mimic the motor activity in living cells. The simplest version contains the particle x of interest and a degree q that mimics the role of an active environment, e.g., motor activity in biological cells. The equations of RHC read³³,

$$\dot{x} = -\frac{k}{\gamma}(x - q) + \xi_x, \quad (4a)$$

$$\dot{q} = \xi_q, \quad (4b)$$

with white noises $\langle \xi_i(t) \xi_j(t') \rangle = 2D_i \delta(t - t') \delta_{ij}$ and $i, j \in \{x, q\}$. In Eq. (4), the coupling between x and q is non-reciprocal, i.e., while the particle x is subject to a force $-k(x - q)$ with a force constant k , the dynamics of q is independent of x . q may thus be seen as a (diffusing) motor that is so strong ("strong as a horse")

that it does not feel the presence of the particle. The system of Eqs. (4) is a two dimensional Gaussian process. Due to the mentioned non-reciprocal coupling, it breaks detailed balance for any finite value of D_q ³³. However, the stochastic process x resulting from Eqs. (4) is a one dimensional Gaussian process, which does not break time reversal symmetry^{36,37}. In other words, evaluating MBR_{anti} in Eq. (3) for the process of Eq. (4) must yield a vanishing result.

In order to obtain a process that breaks time reversal symmetry, we thus render the model non-Gaussian, by making the motor dynamics q a discrete symmetric random walk with step length Δq and time interval between steps of \mathcal{T} , see Fig. 1 for a sketch. The equations of the discrete random horse and cart model (dRHC) read for $t > 0$

$$\dot{x} = -\frac{k}{\gamma}(x - q) + \xi_x \quad (5a)$$

$$q = q_0 + \sum_{n=0}^{\text{floor}(\frac{t}{\mathcal{T}})} \epsilon_n \Delta q \quad (5b)$$

with $\langle \xi_x(t) \xi_x(t') \rangle = 2D_x \delta(t - t')$, $\epsilon_n \in \{-1, 1\}$ with symmetric probabilities $p(\epsilon_n = 1) = p(\epsilon_n = -1) = \frac{1}{2}$. The dRHC model is sketched in Fig. 1 where we also show an example trajectory.

As mentioned, dRHC differs in one crucial aspect from RHC in Eq. (4): The resulting process x is non-Gaussian, and potentially allows detection of time reversal symmetry breaking. Additionally, the active driving mechanism in dRHC introduces a driving length scale, allowing to investigate whether MBR allows detection of this scale.

B. MBR and time reversal breaking

Figure 2 a) shows MBR from both forward and reversed trajectories from dRHC, obtained from numerical solution (simulation) of Eq. (5). The blue curve shows the case of zero step length Δq , i.e., the case of a Brownian particle in a stationary potential. In this case, the process of x obeys time reversal symmetry, and MBR approaches $\frac{1}{2}$ ³³. Furthermore, as this case is time reversal symmetric, MBR evaluated from forward and MBR from backward trajectories are identical – the dashed and solid lines are on top of each other. However, for finite step lengths Δq (purple and red curves, see labels), time reversal symmetry is broken: MBR evaluated from forward and backward trajectories differ. This difference grows with the step length Δq .

Figure 2 b) shows MBR_{anti} of Eq. (3), i.e., the difference between solid and dashed curves in Fig. 2, for the same parameters with the same color code. This graph highlights the breaking of time reversal symmetry for the cases with finite Δq .

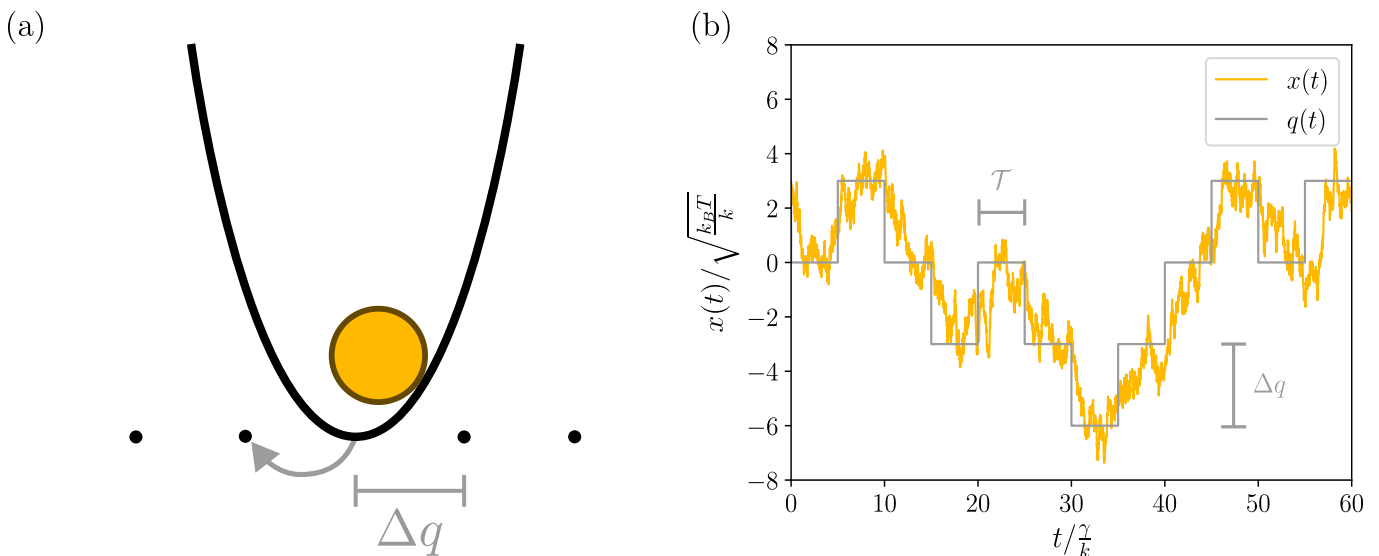


Figure 1. (a) Sketch of the dRHC model of Eq. (5). A Brownian particle is trapped in a harmonic potential whose center performs a discrete random walk with time intervals \mathcal{T} and step length Δq . (b) Shows an example trajectory of x and q for $\Delta q = 3.0\sqrt{\frac{k_B T}{k}}$ and $\mathcal{T} = 5.0\frac{\gamma}{k}$. This illustrates that q performs discrete steps in space and time, while x follows with a delay.

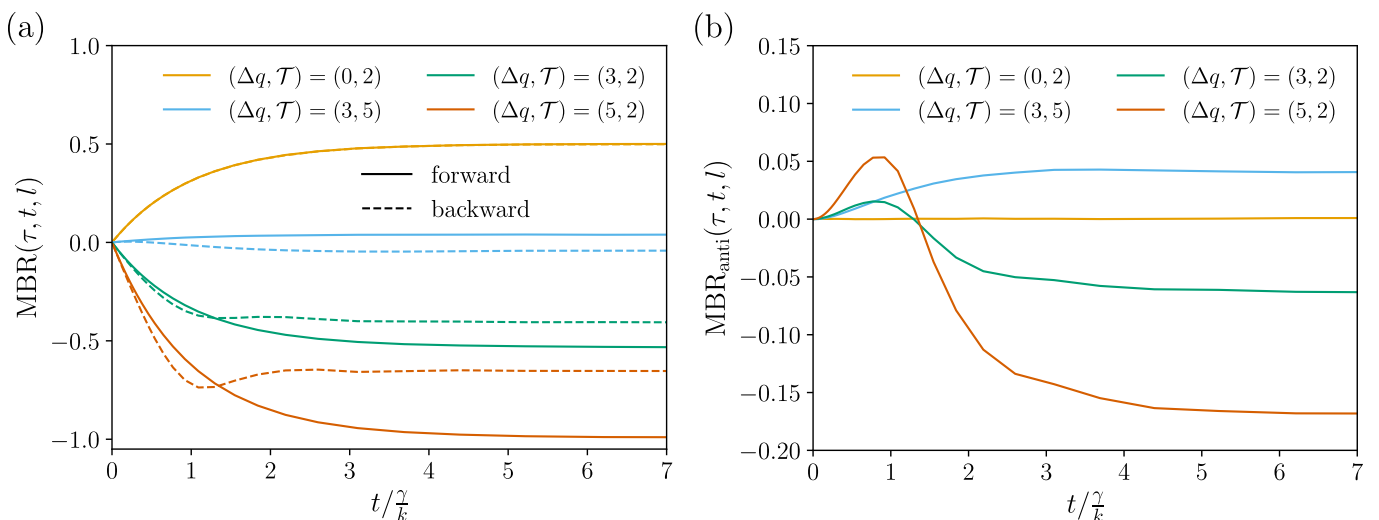


Figure 2. (a) MBR for the dRHC model of Eq. (5) as a function of time t for $\tau = \frac{\gamma}{k}$, $l = 0.01\sqrt{\frac{k_B T}{k}}$ and $(\Delta q, \mathcal{T}) \in \{(0, 2), (3, 5), (3, 2), (5, 2)\}$ with Δq in units of $\sqrt{\frac{k_B T}{k}}$ and \mathcal{T} in units of $\frac{\gamma}{k}$. Solid (dashed) lines: MBR from forward (backward) trajectories. Differences between solid and dashed signal time reversal symmetry breaking. Blue lines show the case of $\Delta q = 0$ (equilibrium), and solid dashed are on top of each other. (b) MBR_{anti} of Eq. (3) for the same parameters, i.e., difference between solid and dashed lines of panel a).

C. Dependence on length and time scales

The model of Eq. (5) is driven by the active process q with inherent time scale \mathcal{T} and length scale Δq . Can we extract these scales in MBR evaluated for x ? We will discuss this question in this subsection, to be later able to address it in case of living cells.

Figure 3 presents the anti-symmetric component of long-time MBR, i.e., $\text{MBR}_{\text{anti}}(\tau, t \rightarrow \infty, l)$ of Eq. (3),

for the dRHC model of Eq. (5), for fixed model parameters, as a color map across the MBR-parameters τ and l . This visualization reveals a striking observation: The map shows a periodic structure of alternating maxima and minima. This periodicity is visible in both the τ and l directions. Even more striking: The distance between successive peaks along the τ direction corresponds very precisely to the interval of the non-equilibrium driving, namely \mathcal{T} : The dashed gray lines, added as guide to the

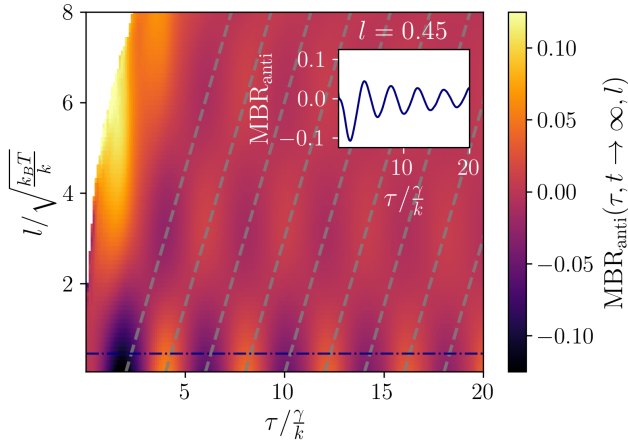


Figure 3. Anti-symmetric part of MBR, i.e., MBR_{anti} of Eq. (3), for trajectories from dRHC model of Eq. (5) as functions of τ and l . Model parameters are $\Delta q = 3\sqrt{\frac{k_B T}{k}}$ and $\mathcal{T} = 2.0\frac{\gamma}{k}$. Gray lines are guides to the eye, and they follow Eq. (6). Horizontal distance between neighboring dashed lines is \mathcal{T} , vertical distance is Δq . This allows extraction of the active time and length scale. Inset shows MBR_{anti} as a function of τ for $l = 0.45\sqrt{\frac{k_B T}{k}}$ (indicated by dash-dotted line in main graph), illustrating the oscillatory nature.

eye, have exactly horizontal distances of \mathcal{T} .

The vertical separation observed in Fig. 3 corresponds, again very precisely, to Δq : The vertical distance between neighboring grey dashed lines is given by Δq . Precisely, the gray dotted lines follow

$$l(\tau) = \frac{\Delta q}{\mathcal{T}} (\tau - n \cdot \mathcal{T}) \quad (6)$$

with $n \in \mathbb{N}$.

The striking finding of Fig. 3, with Eq. (6), is a strong indication that the length and time scales of non-equilibrium mechanisms can indeed be distilled via MBR.

The discrete random horse and cart model has a sharp step interval of \mathcal{T} , which gives rise to the sharp and pronounced features of Fig. 3. To test the robustness of this finding against some randomness in the step interval, we now take the jump interval from a Gaussian distribution with mean \mathcal{T} and a variance of σ_t . Fig. 4 mirrors Fig. 3 in all parameters, except for the randomly drawn step interval with a value of $\mathcal{T}/\sigma_t = 4$. The overall structure of the figure is similar to Fig. 3, i.e., the oscillatory structure quantified by Eq. (6) is visible. However, as may be expected, the structure is more washed out, and the amplitude of the peaks diminishes with larger values of τ and l . We conclude that, as expected, variability in the driving process makes it harder to extract length and time scales via MBR.

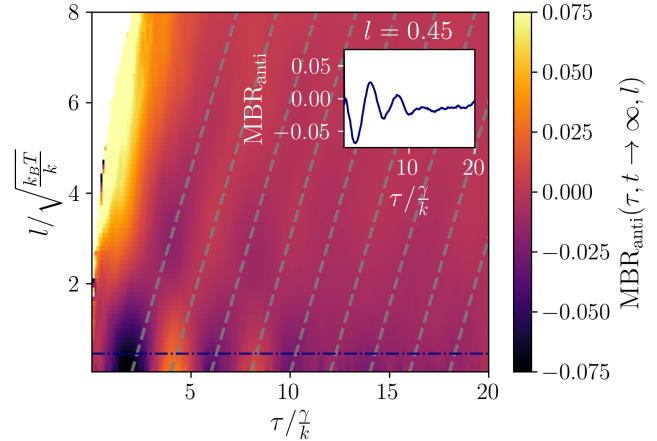


Figure 4. Anti-symmetric part of MBR, i.e., MBR_{anti} of Eq. (3), for dRHC of Eq. (5), with all parameters identical to Fig. 3, but with Gaussian distributed step intervals with standard deviation $\sigma_t/\mathcal{T} = 1/4$. Gray lines are guides to the eye, and they follow Eq. (6), i.e., horizontal distance between neighboring dashed lines is \mathcal{T} , vertical distance is Δq . Inset shows MBR_{anti} as a function of τ for $l = 0.45\sqrt{\frac{k_B T}{k}}$ (indicated by dash-dotted line in main graph), illustrating the decaying oscillatory nature.

IV. TRAJECTORIES FROM LIVING CELLS

In this section, we analyze trajectories of probe particles in living cells^{27,33}, using the tools developed and tested for the dRHC model in Section III. The cell types used are human epithelial lung cancer cells (A549), mouse metastatic lung cancer cells (CT26), mouse immune cells derived from immortalized bone marrow cells where differentiation is controlled by repressing the HoxB8 gene (HoxB8) and human cervical cancer cells untreated (HeLa), as well as HeLa cells treated with both, cytochalasin B and nocodazole, to depolymerize the actin and the microtubule network respectively (drugged).

A. Time reversal breaking

We investigated MBR curves from trajectories obtained in living wild type and passivated cells in previous works^{33,35}. We observed astonishing relations between MBR and effective energies, the latter quantifying breakage of the fluctuation dissipation theorem³³. However, the breakage of detailed balance of trajectories recorded in cells has, to our knowledge not been demonstrated.

Figure 5 a) shows MBR evaluated for various cell types, as a function of time. We observe clear and pronounced differences between MBR evaluated from forward and backward trajectories, demonstrating a breaking of time reversal symmetry. In contrast, for the drug-treated HeLa cells, there is no difference between forward and

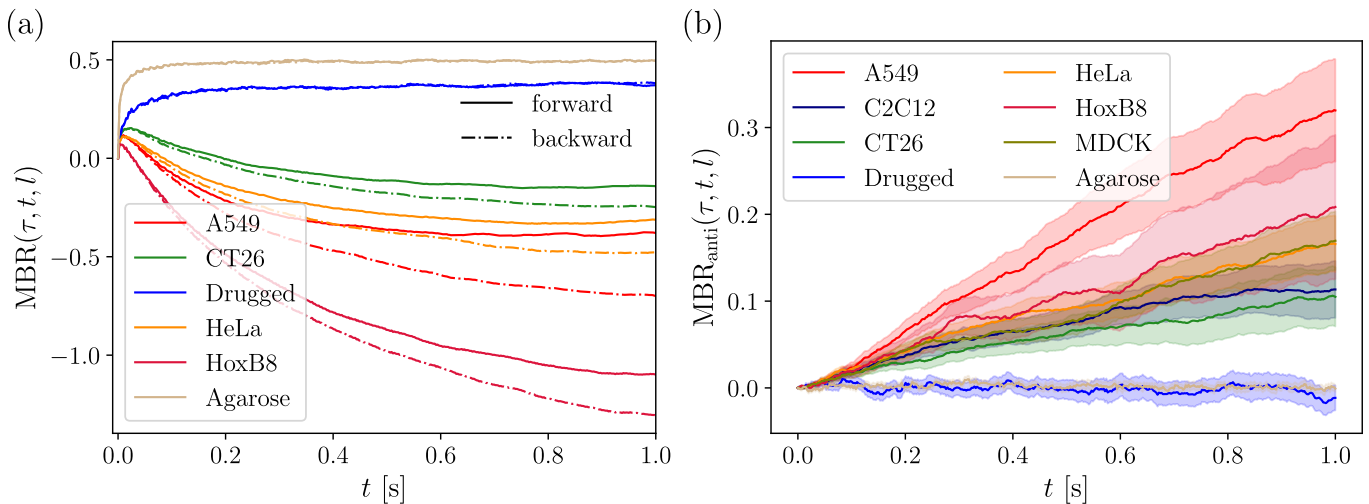


Figure 5. (a) MBR for various cell types, as labelled, for $\tau = 0.047\text{s}$ and $l = 0.002\mu\text{m}$. Solid lines show MBR evaluated for time-forward trajectories and dotted lines for time-backward trajectories. For the wild-type cells, the solid and dotted lines disagree, indicating a breakage of time reversal symmetry. For the drug-treated HeLa cells, there is no significant difference between forward and backward curves. (b) Anti-symmetric part of MBR of Eq. (3), i.e., difference between respective dashed and solid lines in (a). Colored envelopes give the standard deviation of a bootstrap distribution (4000 samples). a) and b) also show MBR from trajectories of a probe particle in the purely passive medium of aragose, as a reference.

back cases, i.e., breakage of time reversal symmetry cannot be detected via MBR in these cells.

Figure 5 b) shows the difference between the curves in a), namely the antisymmetric part defined in Eq. (3). In this curve, we also provide error areas, corresponding to the standard deviation obtained by bootstrap analysis. The finiteness of MBR_{anti} is thus statistically significant, i.e., larger than error bars, and we can claim to have demonstrated or detected the breakage of detailed balance in these living cells. For the drugged cell, the value of MBR_{anti} includes zero within error, and no significant breakage of time reversal symmetry can be claimed.

The mentioned drugs disrupt actin and microtubules, reducing cytoskeletal motor activity, which likely explains the absent time reversal breaking in these cells.

Fig. 5 a) and b) also include trajectories from probe particles in agarose, a purely passive medium. the behavior of MBR is similar to the one in the drugged cell, i.e., no breakage of time reversal symmetry is found.

B. Dependence on length and time scales

In Fig. 6 we show MBR_{anti} at $t = 1\text{s}$, as functions of τ and l , for HoxB8 (a) and HeLa (b) cells, in close resemblance of Fig. 3. Both figures show peak structures, indeed similar to Fig. 3, however washed out, the more so for the case of HeLa. Comparing to Fig. 3, this periodicity suggests active length and time scales of roughly 500 ms and 20 nm, respectively, in both cell types. The insets in Fig. 6 show MBR_{anti} as a function of τ for a fixed l , indicating another peak at around 100 ms or below. Figure 11 in Section A shows the same for the other

untreated cells where we also observe washed out peaks. The particle trajectories analyzed here report the motion of phagocytosed polystyrene beads with a diameter of $1\mu\text{m}$. At the time of recording, these non-degradable particles represent membrane-covered rigid objects that are stored in the cell similarly to lysosomes. Lysosomes are typically transported inside cells by microtubule-based motors, such as kinesins or dynein, which can operate in a tug-of-war configuration.

Given the complexity of the cytosol and our observation that these particles do not move processively once they are close to their destination, characteristic timescales on the order of 100–500 ms are very reasonable^{38,39}. Furthermore, kinesin motors are known to exhibit step sizes of approximately 8 nm, while dynein can often skip binding sites on the microtubule lattice, leading to step lengths of up to 32 nm.

Comparison with the observed cellular data therefore suggests that kinesins, dyneins, or a combination of both could represent the underlying molecular origin of the observed MBR structure. Overall, the approach predicts that dynein is the dominant source of non-equilibrium activity, as it better matches the observed length and timescales. This suggests that polymerization of microtubules should have a stronger effect on the observed peaks than depolymerizing actin⁴⁰.

The maps for both cells however show a feature not visible for the dRHC model of Fig. 3: On the left hand side of the maps, there is an area of pronounced negative MBR_{anti} values. This will be discussed in the next subsection, where we show these on time logarithmic axes.

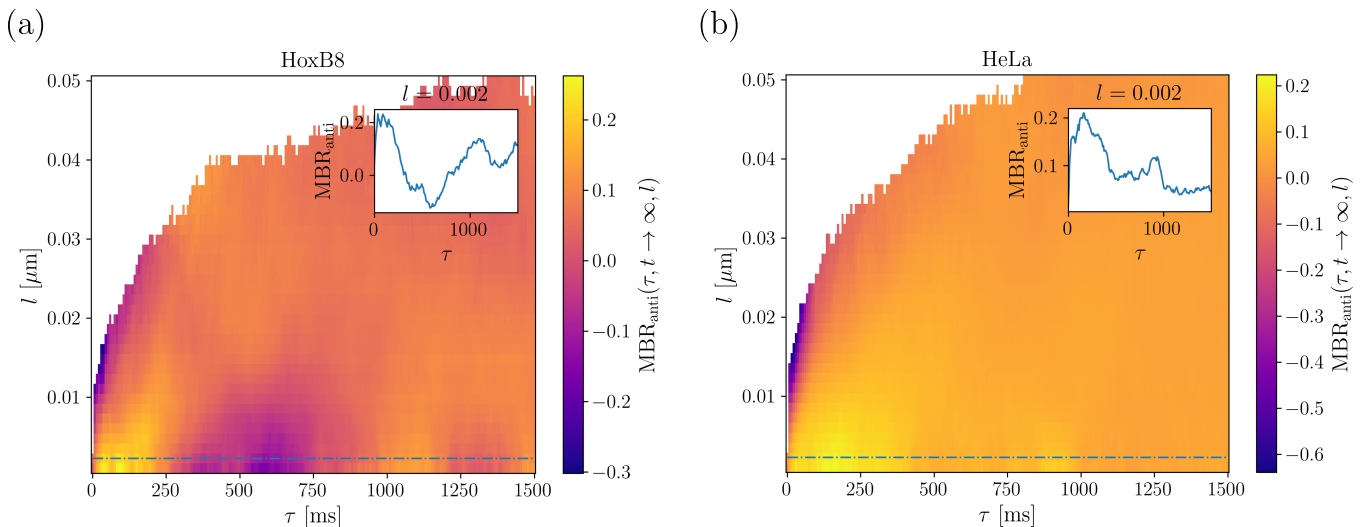


Figure 6. MBR_{anti} at $t = 1$ s as functions of τ and l for (a) HoxB8 and (b) HeLa cells. The periodic structure of Fig. 3 is notable, however washed out. From the periodicity, we estimate the time and length scales to roughly 500 ms and 20 nm, respectively, in both cell types. Insets show MBR_{anti} as functions of τ for fixed l (i.e., along the dash-dotted lines in the main graphs), indicating another timescale at around 100 ms or below.

C. Drugging HeLa Cells

In Fig. 7, we show the anti-symmetric part of MBR at $t = 1$ s for multiple HeLa cell variants, each as functions of τ and l . Fig. 7 is similar as Fig. 6, but using an logarithmic τ axis, and comparing different stages of drugging. Fig. 7a) shows the wild type case, i.e., this map shows identical data as Fig. 6b), except presented on a logarithmic τ axis. As expected, the periodicity discussed around Figs. 3 and 6 is not evident in the logarithmic representation. However, this representation emphasized the strongest antisymmetric signal that is found just at the border of the detectable regime. This signal corresponds to a length scale of 10 – 20nm and a timescale of 5 – 50ms. Indeed these scale correspond perfectly to the expected signal from dynein motor proteins.

As dynein is a microtubule based motor protein, we systematically disrupted either microtubules, actin filaments, or both. If our hypothesis that the anti-symmetric signature indeed corresponds to dynein, then we expect a strong effect when depolymerizing microtubules, and a less strong effect when disrupting the actin cytoskeleton. Indeed as shown in Fig. 7b), HeLa cell with actin removed by drugging with CytoB still have a persisting time reversal breaking. Although the amplitude or extent of reversal breaking is slightly reduced, this implies that actin is not crucial for the processes breaking time reversal. In contrast, when depolymerizing the microtubules using Nocodazole (Fig. 7 c) no time reversal breaking is notable in the MBR, implying that microtubules are important for the cell’s active processes. This is further confirmed when disrupting both, actin filaments and microtubules (Fig. 7 d) which resembles the situation of only removing microtubules. This analysis suggests that the time

reversal breaking is mainly linked to active processes related to the microtubules, and is consistent with the hypothesis that the main force generating motor protein is dynein.

V. BOUND FOR ENTROPY PRODUCTION

A. General: Entropy bound from MBR

Can we quantify the breaking of time reversal symmetry in the investigated cells? To answer this question we consider a path observable $O[\omega]$ that depends on the path ω in phase space, with path probability $p[\omega]$. The average of this observable is formally given by the sum over paths⁴¹ $\langle O \rangle = \int \mathcal{D}\omega O[\omega] p[\omega]$. To quantify the mentioned path reversal properties, we resort to the stochastic change in entropy defined as the log ratio of path probabilities^{42–44}

$$s = \log \frac{p[\omega]}{p[\theta\omega]}. \quad (7)$$

We use notation for path reversal, $\theta\omega$, including reversal of time as well as of kinematic reversal of momenta⁴⁵. For simplicity, we will in the following refer to s as the entropy production (formally per Boltzmann constant k_B), despite some caveats regarding this term⁴⁶.

We will use s in Eq. (7) as a quantifier of broken time reversal symmetry and activity in the investigated cells. Specifically, we will make use of the following inequality, or bound²⁷

$$\langle s \rangle \geq \langle O_a \rangle \log \left(\frac{1 + \langle O_a \rangle}{1 - \langle O_a \rangle} \right). \quad (8)$$

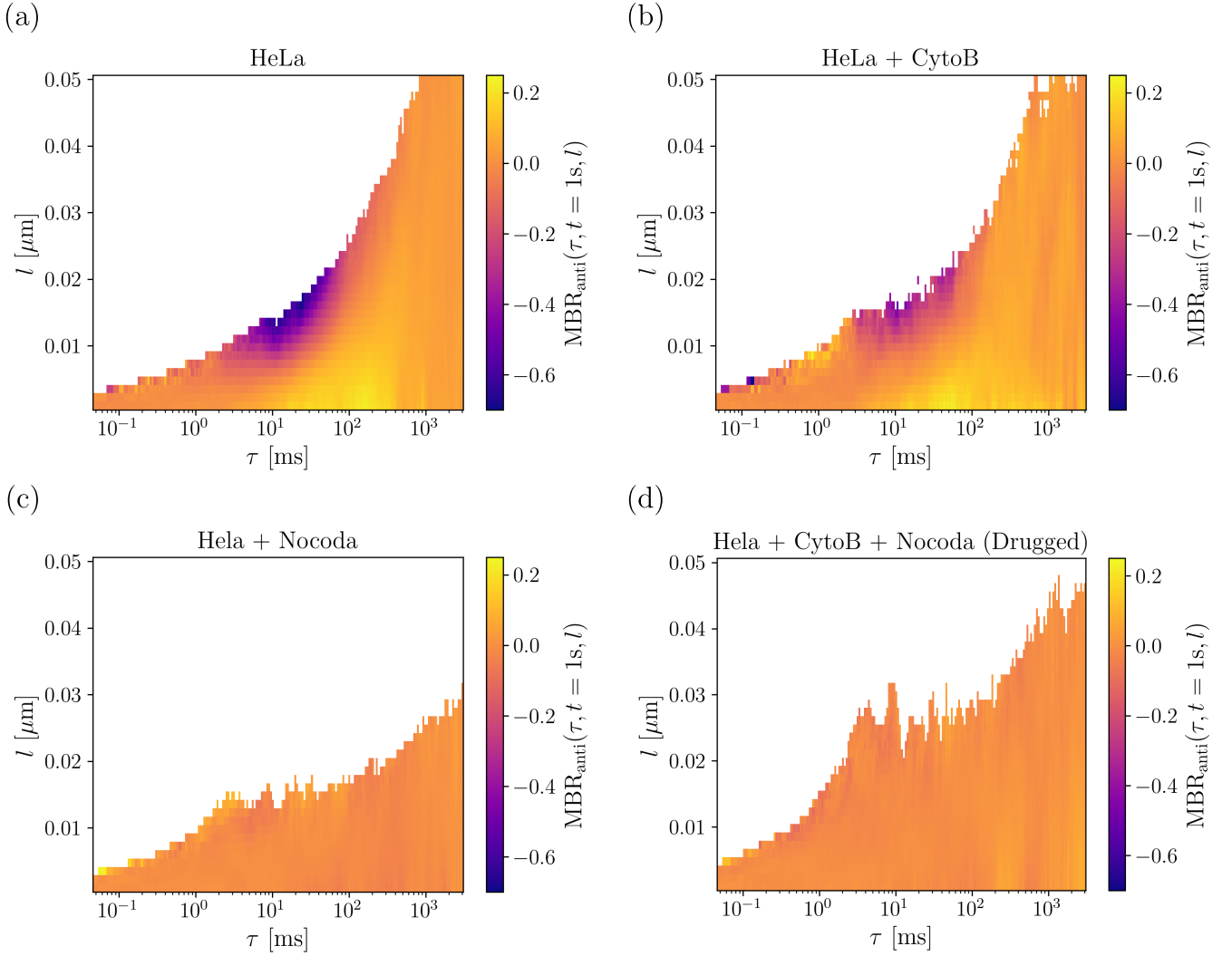


Figure 7. Anti-symmetric part, MBR_{anti} at $t = 1$ s as functions of τ and l for HeLa cells treated with different drugs. In white areas insufficient amount of events was recorded to generate a reliable average value, which is at the base of the MBR approach. (a) Wild type, i.e., undrugged cell. (b) Drugged with Cytochalasin B (CytoB), a drug that removes actin. (c) Drugged with Nocodazole (Nocoda), a drug that disrupts microtubules. (d) Drugged with both CytoB and Nocoda. Case d) is referred to as the "drugged case" of Fig. 5.

Eq. (8) provides a bound for entropy production $\langle s \rangle$ based on any anti-symmetric observable $O_a[\omega] = -O_a[\theta\omega]$ with $|O_a| \leq 1$. Eq. (8) can be used with MBR_{anti} as a basic anti-symmetric observable, as shown below, where we focus on the sign of MBR_{anti} . Furthermore, Eq. (8) is based on a fluctuation theorem²⁷, and hence enjoys broad validity.

Specifically, we express O_a in terms of the antisymmetric part of MBR,

$$O_a(\tau, t, l) = \text{sign} \left(-\frac{x(t+\tau) - x(\tau)}{x(\tau) - x(0)} \vartheta_l(x(\tau) - x(0)) + \frac{x(0) - x(t)}{x(t) - x(t+\tau)} \vartheta_l(x(t) - x(t+\tau)) \right). \quad (9)$$

The antisymmetric observable chosen in Eq. (9) is based on the observable averaged over in MBR_{anti} in Eq. (3), with an additional operation of sign, to ensure $|O_a| \leq 1$. The parameters τ , l and t may now be varied in Eq. (9) to maximize the bound in Eq. (8).

B. Entropy bound from dRHC model

Figure 8 shows the right hand side of Eq. (8) using the observable Eq. (9) applied to the dRHC model for fixed model parameters Δq and \mathcal{T} as given. The graph shows a color map as functions of τ and $t + \tau$, for a fixed value of $l = 0.05 \sqrt{\frac{k_B T}{k}}$, motivated by Fig. 3.

Figure 8 reveals that the total trajectory length ($t + \tau$)

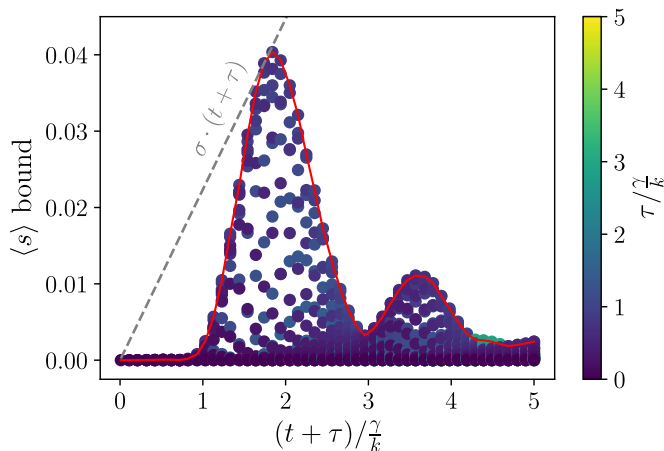


Figure 8. Entropy bound, Eq. (8), using Eq. (9) for the dRHC model of Eq. (5) with $l = 0.05\sqrt{\frac{k_B T}{k}}$, $\Delta q = 5.0\sqrt{\frac{k_B T}{k}}$ and $\mathcal{T} = 1.0\frac{\gamma}{k}$. Each point marks a distinct combination of t and τ adding up to $t + \tau$ on the x -axis, with τ as color coded. Red line shows the maximum of all points as a guide to the eye. Gray dotted line shows the largest bound for entropy production rate σ , with a slope of $\approx 0.022\frac{k}{\gamma}$.

largely dictates the bound on $\langle s(t + \tau) \rangle$, with multiple (t, τ) combinations yielding the same bound. Plotting Fig. 8 as a function of $t + \tau$ lies in extraction of entropy production rate σ . As the process is stationary, we may assume a constant rate σ that yields its bound as

$$\sigma \geq \max_{t, \tau} \frac{1}{t + \tau} \langle O_a(\tau, t, l) \rangle \log \left(\frac{1 + \langle O_a(\tau, t, l) \rangle}{1 - \langle O_a(\tau, t, l) \rangle} \right). \quad (10)$$

The largest bound for σ is thus obtained from drawing a line through the origin with the smallest slope that bounds all points in Fig. 8 from above. This line is shown as a dashed line in Fig. 8. With this procedure, we obtain for the model parameters used in Fig. 8 a bound of $\sigma_{\text{bound}} \approx 0.022\frac{k}{\gamma}$.

To compare the bound with the actual entropy production rate, we numerically compute the work rate performed by the degree q on x , i.e.²²,

$$\begin{aligned} \sigma_{\text{work}} &= \frac{1}{k_B T} \lim_{t \rightarrow \infty} \frac{1}{t} \int_0^t F(x, q) \circ dx(s) \\ &= \frac{1}{k_B T} \lim_{t \rightarrow \infty} \frac{1}{t} \int_0^t -k(x(s) - q(s)) \circ dx(s) \end{aligned} \quad (11)$$

where $\circ dx(a)$ indicates that the integral is taken with Stratonovic convention. This yields, for the same model parameters $\sigma_{\text{work}} \approx 12.265\frac{k}{\gamma}$, significantly larger than the estimated bound for σ . While interesting, this comparison may, at first sight, be considered not very useful, as σ_{work} in Eq. (11) yields the work done, while σ estimated from Fig. 8 is the entropy production from the trajectory of x . Naturally, the latter is smaller, which may also be understood from the above made statements: If

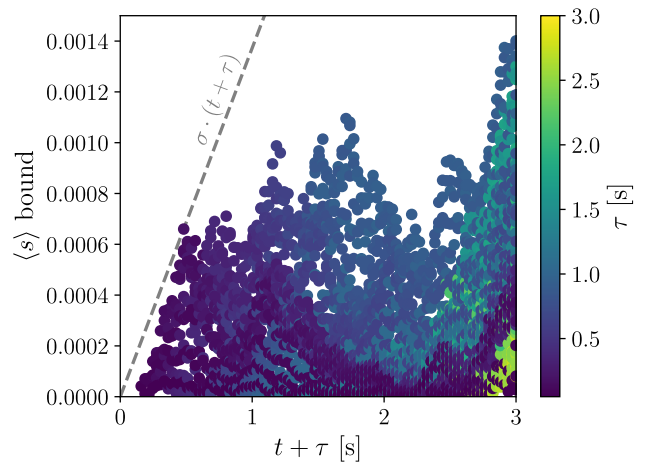


Figure 9. Entropy bound, Eq. (8), using Eq. (9) for HeLa cells with $l = 0.002\mu\text{m}$. Each point marks a distinct combination of t and τ adding up to $t + \tau$ on the x -axis, with τ as color coded. Gray dotted line shows the best bound for entropy production rate σ , with a slope of $\approx 0.0014\frac{1}{s}$.

the process x was Gaussian – as, e.g., in the RHC model of Eq. (4) – the estimate of σ from x would yield zero, while the work done in Eq. (11) would still be finite. It is the non-Gaussianity in x which is needed for a finite estimate from x .

This being said, the comparison is useful, because for the cells investigated below, we face the same issue: We estimate entropy production from a single degree x , which naturally highly underestimates the total number of energetic processes in the cell.

Finally, we aim to point out that the bound obtained from Fig. 8 naturally underestimates the entropy production of the process x – by how much is hard to say, because finding the true value is difficult.

C. Cells

We now turn to the same analysis in cell data. Figure 9 shows the right hand side of Eq. (8) using the observable in Eq. (9), as functions of combinations of t and τ for HeLa cells. We choose a value of $l = 0.002\mu\text{m}$, because, according to Figs. 6 and 7, this value – which is on the edge of experimental resolution – yields large time reversal symmetry breaking. As for the model system we see multiple combinations of (t, τ) yielding the same bound $\langle s(t + \tau) \rangle$. Following the procedure as in Fig. 8 yields a bound for entropy production rate σ .

Figure 10 shows the so obtained bound for σ for all cells investigated. As control measurement, we also show the bound calculated from trajectories of colloidal particle in agarose, a purely passive fluid. Indeed these particles yield the lowest bound for σ , thus providing an idea of the accuracy of this method (see discussion in Section VI

below). For all values, errorbars show the 95% confidence interval of a bias-corrected and accelerated bootstrap. We can see that the error for all cell types is rather large, which may indicate significant variability across different cells of the same cell type, consistent with measurements of active energy in these cells⁴⁰.

The values obtained for entropy production rate are small, and they are not to be understood as the entropy production rate of the cell, see also the discussion for the dRHC model in Section V B. As mentioned there, the reason for this smallness lies in the fact that only a single, one-dimensional degree is observed, and many other important degrees of cell dynamics are not. We remind that if such a single degree is Gaussian, it shows no entropy production at all, i.e., it can only be non-Gaussian features that contribute to σ . This shows the difficulty in estimating entropy production from a suspended particle. Further, Eq. (8) is a bound, and Eq. (9) is not the optimal observable (which is the signum of entropy production²⁷). This implies that the entropy production of the single degree is also likely underestimated in Fig. 10.

Despite these difficulties, do the values of Fig. 10 have a relative meaning between cells? To compare with another activity measure, we recall the effective energy, which quantifies the violation of FDT and was determined for the investigated cells in Refs.^{33,40}, using an optical tweezer setup. It is defined as the ratio^{5,47,48}

$$E_{\text{Eff}}(\omega) = \frac{\omega C(\omega)}{2\chi''(\omega)}, \quad (12)$$

with the power spectral density $C(\omega)$ of the degree x and the imaginary part of the response function $\chi''(\omega)$ of this degree. For the cells investigated here, it was observed that the effective energy follows a power law, i.e., $E_{\text{Eff}}(\omega) \approx k_B T + E_0 \frac{\omega_0}{\omega}$. The prefactor E_0 , determined at $\omega_0 = 1$ Hz, depends on the cell under investigation⁴⁰, and we take it as a measure of the cell's activity.

Figure 10 shows these values of E_0 on the x -axis, i.e., the cells are ordered from left to right according to the measured values of E_0 . This yields monotonically growing values of σ , except for MDCK cells, whose value of σ appears too small relative to the found effective energy. Given the uncertainty in both measures, the curve demonstrates convincingly that the two independent ways of quantifying the cell's activity yield a similar trend and hierarchy.

VI. DISCUSSION

We investigated the breaking of time reversal symmetry in one dimensional stochastic trajectories, both from a driven model as well as from probe particles in living and passivated cells. We demonstrate that the antisymmetric part of the mean back relaxation can detect the mentioned broken time reversal symmetry.

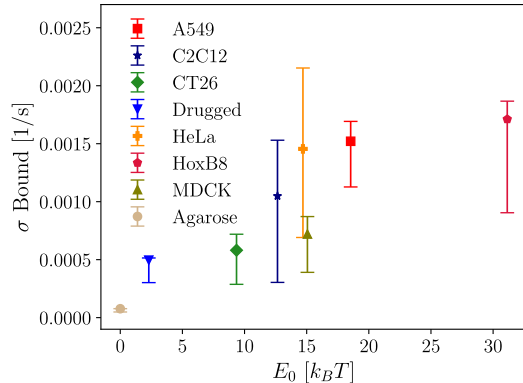


Figure 10. Bound for entropy production rate σ for different cell types and agarose, as extracted from procedures in Fig. 9. Error bars are obtained via bias corrected and accelerated bootstrap (4000 samples) with a confidence interval of 95%. x axis shows the effective energy E_0 , which was determined in Ref. 33, and which quantifies violation of FDT.

To allow for time reversal symmetry breaking, we extend the previously introduced random horse and cart model to a non-Gaussian version, thereby introducing a length and a time scale of driving.

Evaluating time reversal symmetry breaking via MBR for this model reveals that by changing the length and time parameters of MBR, the mentioned length and time scales of model-activity can indeed be observed. Applying the same method to cell data shows very similar features, and we determine the length scale of pronounced breaking of time reversal symmetry to be roughly 10 to 20 nm. As for time scales, there are various signatures, most prominently at around 500 ms, 100 ms and 10 to 100 ms. These observations represent, to our knowledge, the first demonstration of time reversal symmetry breaking with colloidal particles *in vivo*. Previous studies have observed similar effects in *in vitro* systems, such as those utilizing nanotubes³⁰, or for larger systems like hair bundle cells²⁹.

Treating cells by drugs reveals a connection between the observed time reversal breaking and activity of the cytoskeleton, particularly involving microtubules and the motor protein dynein. Other studies have similarly found that anomalous diffusion is greatly reduced if microtubules are depolymerized, but not if actin is destroyed⁴⁹.

To quantify breaking of time reversal symmetry, we employ a bound expression for entropy production rate, for both the model as well as for the cell data. For the model, this bound is, as expected, much smaller than the work performed by activity. We re-emphasize a natural difficulty in extracting entropy production from a reduced set of observables. This is especially so for a one dimensional trajectory, as it requires non-Gaussianity for a finite time reversal symmetry breaking. Despite these

challenges, we convincingly extract entropy production from cell data, which is in astonishing qualitative agreement to previously determined effective energies.

We note another challenge in extracting entropy production from noisy data exemplified for the passive aragose: While the antisymmetric part of MBR in Fig. 5 b) fluctuates around zero for aragose, the entropy bound expression Eq. (8) is inherently non-negative, and systematic instrument noise, like drifts will induce a finite entropy production bound, as seen in Fig. 10, where the value of aragose is finite within error. This hints at a general difficulty when employing entropy bounds with experimental (noisy) data.

There are various possibilities for future work: It will be important to identify the effects of specific motor proteins and observing their influence on the time and length scales appearing in time reversal symmetry breaking. It may also be interesting to investigate further the observed relation between entropy production and violation of fluctuation dissipation theorem. Such relationship may indeed be motivated by the Harada-Sasa relation, which relates, for a simple Langevin equation, the integral over FDT violation to entropy production⁹. Finally, one may incorporate explicit modeling of the underlying Markov chains governing the active process⁵⁰.

REFERENCES

- ¹C. Battle, C. P. Broedersz, N. Fakhri, V. F. Geyer, J. Howard, C. F. Schmidt, and F. C. MacKintosh, “Broken detailed balance at mesoscopic scales in active biological systems,” *Science*, vol. 352, p. 604–607, Apr. 2016.
- ²I. Santra and M. Krüger, “Forces from coarse-graining nonequilibrium degrees of freedom: exact results,” *Journal of Statistical Mechanics: Theory and Experiment*, vol. 2024, p. 123203, Dec. 2024.
- ³M. Guo, A. J. Ehrlicher, M. H. Jensen, M. Renz, J. R. Moore, R. D. Goldman, J. Lippincott-Schwartz, F. C. Mackintosh, and D. A. Weitz, “Probing the stochastic, motor-driven properties of the cytoplasm using force spectrum microscopy,” *Cell*, vol. 158, no. 4, pp. 822–832, 2014. Publisher: Elsevier.
- ⁴H. Turlier, D. A. Fedosov, B. Audoly, T. Auth, N. S. Gov, C. Sykes, J.-F. Joanny, G. Gompper, and T. Betz, “Equilibrium physics breakdown reveals the active nature of red blood cell flickering,” *Nat. Phys.*, vol. 12, pp. 513–519, May 2016.
- ⁵W. W. Ahmed, E. Fodor, M. Almonacid, M. Bussonnier, M.-H. Verlhac, N. Gov, P. Visco, F. v. Wijland, and T. Betz, “Active Mechanics Reveal Molecular-Scale Force Kinetics in Living Oocytes,” *Biophysical Journal*, vol. 114, no. 7, p. 1667–1679, 2018.
- ⁶I. D. Stoev, M. Bolger-Munro, A. Minopoli, S. Wagner, V. R. Krishnaswamy, E. Erben, K. Weißenbruch, N. Maghelli, M. Bastmeyer, C.-P. Heisenberg, and M. Kreysing, “Active and Probe-Free Intracellular Rheology via Phase-Sensitive Thermoviscous Flows,” *bioRxiv*, Apr. 2025.
- ⁷R. Kubo, “The fluctuation-dissipation theorem,” *Reports on Progress in Physics*, vol. 29, p. 255, Jan. 1966.
- ⁸G. S. Agarwal, “Fluctuation-dissipation theorems for systems in non-thermal equilibrium and applications,” *Zeitschrift für Physik A Hadrons and nuclei*, vol. 252, p. 25–38, Feb. 1972.
- ⁹T. Harada and S.-i. Sasa, “Equality Connecting Energy Dissipation with a Violation of the Fluctuation-Response Relation,” *Physical Review Letters*, vol. 95, p. 130602, Sept. 2005.
- ¹⁰T. Speck and U. Seifert, “Restoring a fluctuation-dissipation theorem in a nonequilibrium steady state,” *Europhysics Letters (EPL)*, vol. 74, p. 391–396, May 2006.
- ¹¹M. Baiesi, C. Maes, and B. Wynants, “Fluctuations and response of nonequilibrium states,” *Physical Review Letters*, vol. 103, p. 010602, July 2009. arXiv:0902.3955 [cond-mat].
- ¹²M. Krüger and M. Fuchs, “Fluctuation Dissipation Relations in Stationary States of Interacting Brownian Particles under Shear,” *Phys. Rev. Lett.*, vol. 102, p. 135701, Mar. 2009.
- ¹³M. Baiesi and C. Maes, “An update on the nonequilibrium linear response,” *New Journal of Physics*, vol. 15, p. 013004, Jan. 2013.
- ¹⁴B. E. Vos, T. M. Muenker, and T. Betz, “Characterizing intracellular mechanics via optical tweezers-based microrheology,” *Curr. Opin. Cell Biol.*, vol. 88, p. 102374, June 2024.
- ¹⁵K. Nishizawa, M. Bremerich, H. Ayade, C. F. Schmidt, T. Ariga, and D. Mizuno, “Feedback-tracking microrheology in living cells,” *Sci. Adv.*, vol. 3, p. e1700318, Sept. 2017.
- ¹⁶H. Ebata, K. Umeda, K. Nishizawa, W. Nagao, S. Inokuchi, Y. Sugino, T. Miyamoto, and D. Mizuno, “Activity-dependent glassy cell mechanics i: Mechanical properties measured with active microrheology,” *Biophys. J.*, vol. 122, pp. 1781–1793, May 2023.
- ¹⁷R. K. P. Zia and B. Schmittmann, “Probability currents as principal characteristics in the statistical mechanics of non-equilibrium steady states,” *Journal of Statistical Mechanics: Theory and Experiment*, vol. 2007, p. P07012–P07012, July 2007.
- ¹⁸S. Thapa, D. Zaretzky, R. Vatash, G. Gradziuk, C. Broedersz, Y. Shokef, and Y. Roichman, “Nonequilibrium probability currents in optically-driven colloidal suspensions,” *SciPost Physics*, vol. 17, p. 096, Oct. 2024.
- ¹⁹F. Mori, S. N. Majumdar, and G. Schehr, “Time to reach the maximum for a stationary stochastic process,” *Phys. Rev. E*, vol. 106, p. 054110, Nov 2022.
- ²⁰D. J. Evans, E. G. D. Cohen, and G. P. Morriss, “Probability of second law violations in shearing steady states,” *Physical Review Letters*, vol. 71, p. 2401–2404, Oct. 1993.
- ²¹C. Maes and K. Netočný, “Time-Reversal and Entropy,” *Journal of Statistical Physics*, vol. 110, p. 269–310, Jan. 2003.
- ²²U. Seifert, “Stochastic thermodynamics, fluctuation theorems and molecular machines,” *Reports on Progress in Physics*, vol. 75, p. 126001, Nov. 2012. Publisher: IOP Publishing.
- ²³A. C. Barato and U. Seifert, “Thermodynamic Uncertainty Relation for Biomolecular Processes,” *Physical Review Letters*, vol. 114, p. 158101, Apr. 2015.
- ²⁴J. M. Horowitz and T. R. Gingrich, “Thermodynamic uncertainty relations constrain non-equilibrium fluctuations,” *Nature Physics*, vol. 16, p. 15–20, Jan. 2020.
- ²⁵Y. Hasegawa and T. Van Vu, “Fluctuation Theorem Uncertainty Relation,” *Physical Review Letters*, vol. 123, p. 110602, Sept. 2019.
- ²⁶C. Dieball and A. Godec, “Direct Route to Thermodynamic Uncertainty Relations and Their Saturation,” *Physical Review Letters*, vol. 130, p. 087101, Feb. 2023.
- ²⁷G. Knotz, T. M. Muenker, T. Betz, and M. Krüger, “Entropy bound for time reversal markers,” *Frontiers in Physics*, vol. 11, Feb. 2024. Publisher: Frontiers.
- ²⁸U. Seifert, “From Stochastic Thermodynamics to Thermodynamic Inference,” *Annual Review of Condensed Matter Physics*, vol. 10, p. 171–192, Mar. 2019.
- ²⁹E. Roldan, J. Barral, P. Martin, J. M. R. Parrondo, and F. Jülicher, “Quantifying entropy production in active fluctuations of the hair-cell bundle from time irreversibility and uncertainty relations,” *New Journal of Physics*, vol. 23, p. 083013, Aug. 2021.
- ³⁰A. Bacanu, J. F. Pelletier, Y. Jung, and N. Fakhri, “Inferring scale-dependent non-equilibrium activity using carbon nanotubes,” *Nature Nanotechnology*, vol. 18, p. 905–911, Aug. 2023.
- ³¹C. W. Lynn, E. J. Cornblath, L. Papadopoulos, M. A. Bertolero, and D. S. Bassett, “Broken detailed balance and entropy production in the human brain,” *Proceedings of the National Academy*

- of *Sciences*, vol. 118, p. e2109889118, Nov. 2021.
- ³²For simplicity, we take time reversal symmetry breaking as a measure of non-equilibrium, i.e., excluding cases that may break this symmetry by other means, e.g., magnetic fields⁵¹.
- ³³T. M. Muenker, G. Knotz, M. Krüger, and T. Betz, “Accessing activity and viscoelastic properties of artificial and living systems from passive measurement,” *Nature Materials*, vol. 23, p. 1283–1291, Sept. 2024.
- ³⁴G. Knotz and M. Krüger, “Mean back relaxation for position and densities,” *Physical Review E*, vol. 110, p. 044137, Oct. 2024.
- ³⁵G. Knotz, T. M. Muenker, T. Betz, and M. Krüger, “Evaluating non-equilibrium trajectories via mean back relaxation: Dependence on length and time scales,” *The Journal of Chemical Physics*, vol. 163, p. 124118, Sept. 2025.
- ³⁶G. Weiss, “Time-Reversibility of Linear Stochastic Processes,” *Journal of Applied Probability*, vol. 12, no. 4, p. 831–836, 1975. Publisher: Applied Probability Trust.
- ³⁷R. R. Netz, “Multi-point distribution for gaussian non-equilibrium non-markovian observables,” *arXiv*, 2023. DOI arxiv-2310.08886.
- ³⁸R. Lipowsky and S. Klumpp, “‘Life is motion’: multiscale motility of molecular motors,” *Physica A: Statistical Mechanics and its Applications*, vol. 352, p. 53–112, July 2005.
- ³⁹T. Deguchi, M. K. Iwanski, E.-M. Schentarra, C. Heidebrecht, L. Schmidt, J. Heck, T. Weihs, S. Schnorrenberg, P. Hoess, S. Liu, V. Chevyreva, K.-M. Noh, L. C. Kapitein, and J. Ries, “Direct observation of motor protein stepping in living cells using MIN-FLUX,” 2023.
- ⁴⁰T. M. Muenker, B. E. Vos, and T. Betz, “Intracellular mechanical fingerprint reveals cell type specific mechanical tuning,” May 2024.
- ⁴¹A. Altland and B. D. Simons, *Condensed Matter Field Theory*. Cambridge University Press, 2 ed., 2010.
- ⁴²C. Maes and K. Netočný, “Time-reversal and entropy,” *Journal of Statistical Physics*, vol. 110, no. 1, p. 269–310, 2003.
- ⁴³U. Seifert, “Entropy Production along a Stochastic Trajectory and an Integral Fluctuation Theorem,” *Physical Review Letters*, vol. 95, p. 040602, July 2005.
- ⁴⁴L. P. Fischer, H.-M. Chun, and U. Seifert, “Free diffusion bounds the precision of currents in underdamped dynamics,” *Physical Review E*, vol. 102, p. 012120, July 2020.
- ⁴⁵R. E. Spinney and I. J. Ford, “Entropy production in full phase space for continuous stochastic dynamics,” *Physical Review E*, vol. 85, p. 051113, May 2012.
- ⁴⁶The entropy defined in Eq. (7) corresponds to the total change in entropy in overdamped stationary systems. In underdamped or non-stationary systems the boundary terms differ⁴⁴.
- ⁴⁷P. Martin, A. J. Hudspeth, and F. Jülicher, “Comparison of a hair bundle’s spontaneous oscillations with its response to mechanical stimulation reveals the underlying active process,” *Proceedings of the National Academy of Sciences*, vol. 98, p. 14380–14385, Dec. 2001.
- ⁴⁸N. Narinder and E. Fischer-Friedrich, “Time irreversibility, entropy production and effective temperature are independently regulated in the actin cortex of living cells,” Mar. 2025. arXiv:2503.17016 [physics].
- ⁴⁹A. Sabri, X. Xu, D. Krapf, and M. Weiss, “Elucidating the Origin of Heterogeneous Anomalous Diffusion in the Cytoplasm of Mammalian Cells,” *Physical Review Letters*, vol. 125, p. 058101, July 2020.
- ⁵⁰C. Maes and M. H. van Wieren, “A Markov Model for Kinesin,” *Journal of Statistical Physics*, vol. 112, p. 329–355, July 2003.
- ⁵¹R. Kubo, M. Toda, and N. Hashitsume, *Statistical Physics II: Nonequilibrium Statistical Mechanics*, vol. 31. Springer Science & Business Media, 2012.

Appendix A: Additional graphs from cell data

The experimental details can be found in Ref. 33. Multiple trajectories for different cells and media have been recorded A549 ($N = 179$), C2C12 ($N = 177$), CT26 ($N = 173$), Drugged ($N = 75$), HeLa ($N = 231$), HoxB8 ($N = 170$), MDCK ($N = 183$), Agarose ($N = 27$), HeLa CytoB ($N = 60$) and HeLa Nocoda ($N = 63$) with a sampling time of 1.57×10^{-5} s. For A549, the trajectory lengths lie between 3 s - 10 s with an average of 8.7 s. For HoxB8, the trajectory lengths lie between 5 s - 10 s with an average of 5.6 s. For all other cells and media, the trajectory lengths are exactly 10 s. The anti-symmetric MBR value at $t = 1$ s for A549, C2C12, CT26 and MDCK cells can be found in Fig. 11.

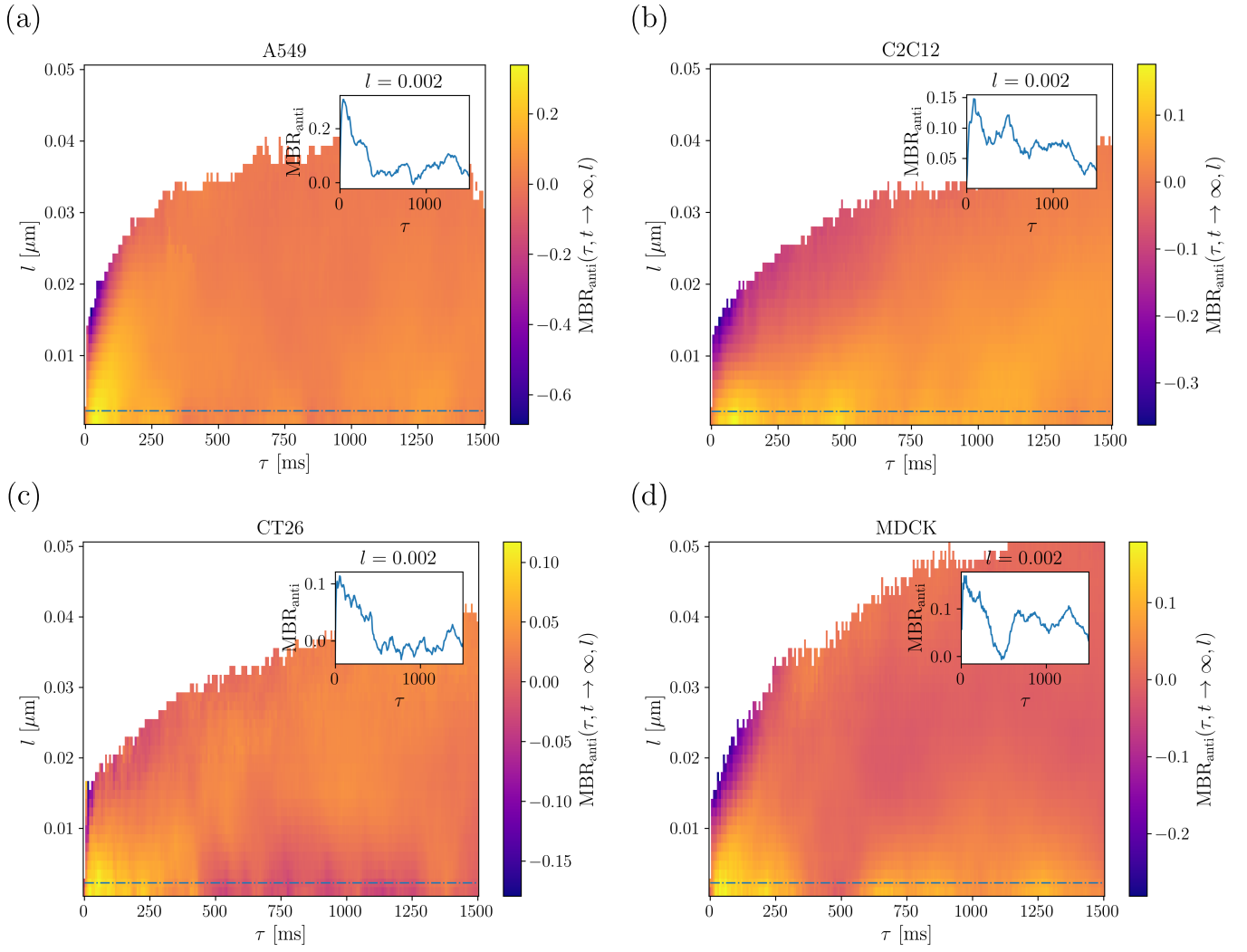


Figure 11. MBR_{anti} at $t = 1$ s as functions of τ and l as in Fig. 6 for (a) A549, (b) C2C12, (c) CT26 and (d) MDCK cells. As in Fig. 6 a washed out periodic structure is notable.